

Molecular dynamics study of the isotropic-nematic quench

Z. Bradač,¹ S. Kralj,^{1,2} and S. Žumer^{2,3}

¹Laboratory Physics of Complex Systems, Faculty of Education, University of Maribor, Koroška 160, 2000 Maribor, Slovenia

²Condensed Matter Physics Department, Jožef Stefan Institute, Jamova 39, 1000 Ljubljana, Slovenia

³Department of Physics, Faculty of Mathematics and Physics, University of Ljubljana, Jadranska 19, 1000 Ljubljana, Slovenia

(Received 21 December 2000; revised manuscript received 6 July 2001; published 22 January 2002)

Effects of cylindrical and spherical confinement on the kinetics of the isotropic-nematic quench is studied numerically. The nematic liquid crystal structure was modeled by a modified induced-dipole–induced-dipole interaction. Molecules were allowed to wander around points of a hexagonal lattice. Brownian molecular dynamics was used in order to access macroscopic time scales. In the bulk we distinguish between the early, domain, and late stage regime. The early regime is characterized by the exponential growth of the nematic uniaxial order parameter. In the domain regime domains are clearly visible and the average nematic domain size ξ_d obeys the dynamical scaling law $\xi_d \sim t^\gamma$. The late stage evolution is dominated by dynamics of individual defects. In a confined system the qualitative change of the scaling behavior appears when ξ_d becomes comparable to a typical linear dimension R of the confinement. In the confining regime ($\xi_d \geq R$) the scaling coefficient γ depends on the details of the confinement and also the final equilibrium nematic structure. The domain growth is well described with the Kibble-Zurek mechanism.

DOI: 10.1103/PhysRevE.65.021705

PACS number(s): 61.30.Cz, 61.30.Jf, 61.30.Pq

I. INTRODUCTION

Kinetics of a system evolving towards the thermal equilibrium phase after a temperature quench of a higher symmetry phase attracts considerable attention of researchers from different fields of science [1–3]. This phenomenon exhibits several universalities and in this respect bridges very different branches of physics. The basic mechanism of the annealing process is in most cases controlled by kinetics of defects [4] (also named vortices, strings, disclinations or dislocations).

One of the simplest systems to study this phenomenon is a temperature quench of a liquid crystal (LC) from the isotropic (I) to the nematic (N) phase. The higher symmetry I phase has properties of an ordinary liquid and does not exhibit any long-range order. The lower symmetry N phase is characterized by the orientational long-range order. The average local orientational ordering is in the continuum picture [5] well described by the uniaxial director field \vec{n} . In thermodynamic equilibrium the director field in the bulk tends to be aligned parallel along the symmetry breaking direction. In a confined nematic LC the equilibrium director profile is in general spatially dependent revealing the balance among elastic, surface, and (eventual) external electric or magnetic field forces. The time evolution of a texture after an I - N quench leading to the equilibrium \vec{n} distribution is realized via a coarse graining process in which defects play an important role.

Defects in a nematic LC correspond to points or lines in space where \vec{n} is not uniquely defined [5,6]. They are classified according to their *topological charge* M that is defined in terms of the director field encircling a defect [5,7,8]. Topologically stable point or line defects have integer and half integer M , respectively. Merging and decaying of defects is controlled by topological conservation laws for which the description of nematic ordering in terms of \vec{n} is sufficient. However, if the core of defects is of interest additional order

parameter fields [5] have to be introduced.

A typical time evolution of a nematic texture after an I - N quench can be qualitatively described in terms of the so-called *Kibble-Zurek mechanism* [3,9], originally introduced to describe symmetry breaking phase transitions in the early Universe. In the early stage of the quench a multidomain structure forms as a result of the broken continuous orientational symmetry [2,3,10–13]. The pattern of these domains (the so-called *protodomains* [3]) results from random thermally induced fluctuations. The average orientational ordering of early stage domains (described by an average orientation of \vec{n} within a domain) is in general uncorrelated in different regions of space. Their typical size is roughly given by the nematic order parameter correlation length ξ_n in the prequench isotropic phase. The texture then gradually evolves into the ground state. The average domain size ξ_d increases with time in a self-similar way exhibiting a scaling behavior.

When studying a rapid I - N quench a density of defects or a domain size ξ_d are monitored [2,10,13]. Both observations yield similar results although domain collision sites do not necessarily give rise to topological defects. Domain walls are mostly nonsingular.

In this contribution computer simulations are used to study quench induced kinetics of a confined nematic LC. Our work was motivated by simulation results obtained by Bhattacharya *et al.* in a continuum-type approach [10]. They studied an I - N quench using a spin-rotor interaction in a parallelepiped pore subject to different anchoring conditions. A typical domain size ξ_d was extracted from the order parameter pair correlation function. The time evolution $\xi_d(t)$, displaying scaling behavior, was governed by the time dependent Ginzburg-Landau equation. They showed that confinement of a typical linear size R gives rise to a change in a scaling relation $\xi_d(t)$ when ξ_d approaches R .

Our interest is to analyze in more detail the influence of confinement on the quench kinetics scaling law. As a confin-

ing geometry we chose the cylindrical tube except in one case where a simulation is carried out in the spherical cavity. The cylindrical geometry is chosen because it reasonable mimics the essential geometrical characteristics of usual confining matrices (i.e., anopore [14] and nucleopore [15] membranes, Vycor glass [16], CPG matrices [17,18]...) of nematic LCs used in several experiments in which LC phase behavior has been studied. In addition this geometry exhibits a rich variety of different equilibrium nematic structures [19] reflecting the interplay among elastic, external field and surface interactions. In our semimicroscopic model LC molecules interact via the modified induced-dipole–induced-dipole-type interaction and are allowed to wander around hexagonal lattice points. The time evolution is realized with the Brownian molecular dynamics [20].

The plan of the paper is the following. The continuum predictions of the phenomena affecting the coarsening dynamics of the nematic texture are presented in Sec. II. In Sec. III we describe our semimicroscopic model. The results of the simulation showing the influence of geometry, structural details, and orientational anchoring conditions on the domain evolution are presented in Sec. IV. In the last section a summary is given.

II. PHENOMENOLOGICAL ESTIMATES

To understand basic mechanisms driving the time evolution of a nematic texture we first carry out some estimates based on the continuum description. For this purpose we limit to the uniaxial nematic ordering [5] described with the nematic director field $\vec{n}(\vec{r})$ and the corresponding order parameter $S(\vec{r})$. The position vector \vec{r} points to a mesoscopic area corresponding to a cluster of LC molecules. The unit vector $\vec{n}(\vec{r})$ points along the average orientation of the local optic axis and $S(\vec{r})$ reflects the fluctuations around it. We neglect biaxial effects that play secondary role in usual nematics [5,11].

In terms of these fields we express the free energy density $f=f_h+f_i$ of the nematic phase using Landau–de Gennes approach [5,19] as

$$f_h = \frac{a}{2}(T-T_*)S^2 - \frac{b}{3}S^3 + \frac{c}{4}S^4, \quad (1a)$$

$$f_i = \frac{L_1}{2}|\vec{\nabla}S|^2 + \frac{L_2}{2}S^2[(\vec{\nabla}\cdot\vec{n})^2 + (\vec{\nabla}\times\vec{n})^2]. \quad (1b)$$

Here f_h and f_i stand for the homogeneous and inhomogeneous contributions, respectively. Note that we include only the essential terms needed to describe qualitatively the phenomena of interest.

The homogeneous term determines the degree of nematic ordering $S=S_b$ in the undistorted bulk nematic phase stable below the phase transition temperature $T=T_{NI}$. In terms of the phenomenological material constants a , b , c , and T_* , it is expressed as $S_b = [b + \sqrt{b^2 + 4ca(T_* - T)}]/2c$. At the temperature $T=T_*$ the isotropic phase ceases to exist even in the metastable state. For most nematics $T_{NI} - T_* \sim 1K$.

The inhomogeneous contribution tends to enforce a spatially homogeneous nematic ordering. The quantities L_i are the nematic bare (temperature independent) elastic constants characterizing the free energy costs of the elastic deformations in S ($i=1$) and \vec{n} ($i=2$). Typically they are of the same order of magnitude. Henceforth, we set $L_1 \sim L_2 \equiv L \sim K/S^2$, where K stands for the average Frank elastic constant [5].

We first estimate the evolution of the nematic ordering developing from a fluctuation in S in the isotropic phase at $T=T_I \sim T_{NI}$ after the quench deep into the nematic phase at $T=T_N = T_I - \Delta T \ll T_{NI}$. We assume that the quench is sudden in time, i.e., short in comparison to relevant nematic order parameter correlation times. The initial fluctuation growth can be described with the time dependent Ginzburg-Landau equation [21] $-\Gamma \partial S / \partial t = \partial f / \partial S$, where the parameter Γ characterizes the dissipation in the system. Taking into account the lowest order term in the free energy expansion [Eq. (1a)] and neglecting the distortion part the fluctuation grows as

$$S(t) \sim S_f e^{t/\tau_0}. \quad (2)$$

Here $\tau_0 = \Gamma / (a\Delta T)$ estimates the nematic order parameter relaxation time at T_N and S_f is the initial fluctuation amplitude in S created at $T \approx T_{NI}$. A substantial degree of ordering is established when the condition $t/\tau_0 \gtrsim 1$ is fulfilled. Above this time [9] the degree of ordering is strong enough so that the domain structure becomes apparent. At this stage the homogeneous free energy contribution f_h is decreased enough to become comparable to f_i .

After domains are established the nematic texture gradually evolves into the ground state. Consequently the average domain size increases with time. In order to understand the basic driving mechanisms of this process we study a motion of an interface (i.e., a domain wall) separating two domains (see Fig. 1) in a three dimensional volume V that we label as A and B , respectively. For simplicity we assume that the domain A is spherical of radius ξ_d and surrounded by the domain B . At a given time the free energy of the observed system is roughly given by $F \sim (4\pi\xi_d^3/3)f_A + [V - (4\pi\xi_d^3/3)]f_B + 4\pi\xi_d^2 d_w f_w$. Here f_A and f_B stand for average free energy densities within domains A and B , respectively. The quantity $f_w \sim L|\nabla\Theta|^2 \sim L/d_w^2$ estimates an average free energy cost to cross the domain wall of width d_w . The angle Θ symbolizes the orientation of the director field and ∇ stands for the gradient operator. In general $f_A \neq f_B$ because of different average director field distortions. Next we assume that the free energy released by the motion of the interface is dissipated, thus

$$-\frac{\partial F}{\partial t} = \int \Gamma \left(\frac{\partial \Theta}{\partial t} \right)^2 dV \sim \Gamma \left(\frac{\partial \Theta}{\partial t} \right)^2 4\pi\xi_d^2 d_w.$$

Assuming

$$\frac{\partial \Theta}{\partial t} \sim |\nabla \Theta| \frac{\partial \xi_d}{\partial t} \sim \frac{1}{d_w} \frac{\partial \xi_d}{\partial t}$$

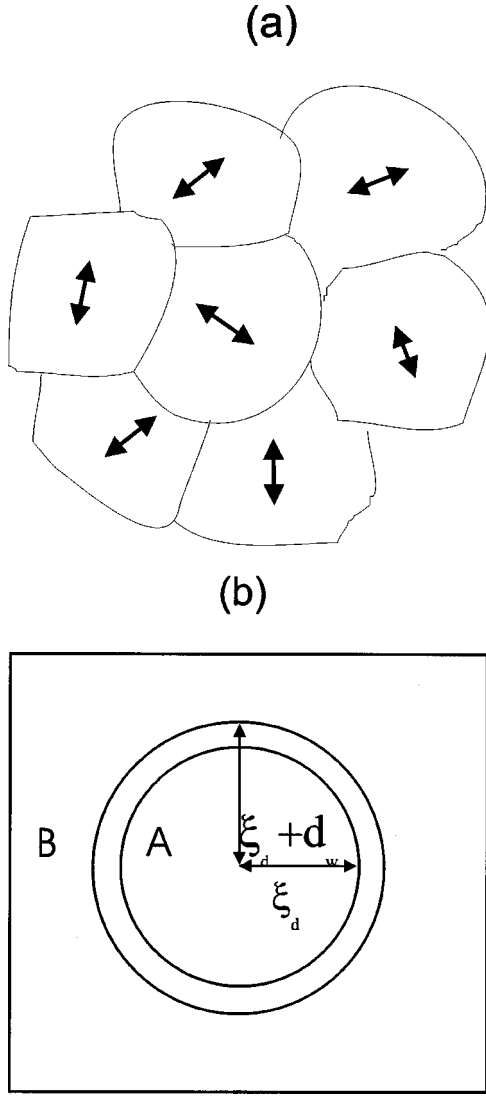


FIG. 1. Schematic presentation of a typical domain structure (a). Average director orientations within domains are depicted by arrows. In (b) the domain geometry used in derivation of Eq. (3) is shown.

one finds, for ξ_d ,

$$\frac{\partial \xi_d}{\partial t} \sim \frac{d_w(f_B - f_A)}{\Gamma} - \frac{L}{\xi_d \Gamma}. \quad (3)$$

The first term tends to enforce $\xi_d \propto t$ if $f_A \neq f_B$. The second term, which tends to reduce the overall domain wall surface, enforces $\xi_d \propto t^{1/2}$.

Note that within the *Kibble-Zurek mechanism* the only source of defects are collision sites of domains. However, the combination of the geometry and the boundary conditions at a domain wall can in principle impose topological constraints yielding defects within domains [8,21,22]. The total topological charge of the director field within the domain is then determined with the Euler characteristics of the enclosing surface. But this constraint comes into the play only if the orientational internal anchoring $W_a^{(\text{intrinsic})}$ (i.e., the anisotropic part of the surface tension) at the domain wall is

strong enough, i.e., $W_a^{(\text{intrinsic})} \xi_d / K \gg 1$. For most liquid crystals this condition requires $\xi_d \gg 0.1 \mu\text{m}$. Thus we believe that this phenomenon does not play a significant role in the coarsening dynamics.

III. MICROSCOPIC MODEL

A. Potential

We model interaction between two rodlike LC molecules placed at \vec{r}_i and \vec{r}_j and oriented along \vec{e}_i and \vec{e}_j , respectively, via a simple modified induced-dipole–induced-dipole pairwise interaction [23,24]

$$f_{ij} = -\frac{J}{r^6} \left[\vec{e}_i \cdot \vec{e}_j - \frac{3\varepsilon}{r^2} (\vec{e}_i \cdot \vec{r})(\vec{e}_j \cdot \vec{r}) \right]^2. \quad (4)$$

Here $\vec{r} = \vec{r}_j - \vec{r}_i$, J is a positive interaction constant, and the dimensionless parameter ε describes the orientational anisotropy. In the continuum picture the thermodynamically averaged value of \vec{e}_i over a small volume located at \vec{r}_i defines the nematic director field $\vec{n}(\vec{r}_i)$. Case $\varepsilon = 0$, known also as the Lebwohl-Lasher or the lattice Maier-Saupe model, corresponds to the so-called equal Frank elastic constants approximation in the continuum description. This refers to the case $K_{11} = K_{22} = K_{33} = K_{24} \equiv K$, $K_{13} = 0$, where K_{11} , K_{22} , K_{33} , K_{24} , and K_{13} stand for the splay, twist, bend, saddle-splay, and splay-bend constant, respectively. For $\varepsilon \neq 0$ the elastic constants are no more equal. Some further properties of this model are given in [24,25]. It reasonably describes properties of nematic liquid crystals for $\varepsilon \leq 0.3$.

At the confining surface we assume strong orientational anchoring [26]. Therefore, at the surface nematic molecules are strictly aligned along the direction preferred by surface interactions.

Note that in our description a *molecule* in fact corresponds to a cluster of N_c molecules [25,27,28], where N_c is believed to range between 1 and $N_n + 1$. The number N_n counts *molecular* sites within a sphere of radius a_0 describing the lattice constant of the hexagonal lattice used in our simulations.

The interaction energy W_{int} of the whole sample is given as a sum over all pair interactions. In calculations we limit to the sum over neighbors within a sphere of radius $r_n = 2.5a_0$, corresponding to approximately 100 pairs. Testing examples indicate that increasing r_n above this value does not affect the simulation results within our accuracy. We also limit to relatively low temperatures, where W_{int} and the free energy F are almost equal.

B. Parametrization and Brownian molecular dynamics

In this contribution we concentrate on a nematic LC confined to a cylindrical cavity with the symmetry axis along the z axis. This suggests the following parametrization of the *molecular* orientation in the laboratory frame:

$$\vec{e}_i = \vec{e}_x \sin \Theta \cos \Phi + \vec{e}_y \sin \Theta \sin \Phi + \vec{e}_z \cos \Theta. \quad (5)$$

The angles $\Theta = \Theta(\vec{r}_i, t)$ and $\Phi = \Phi(\vec{r}_i, t)$ are the variational parameters given at a discrete time t and position $\vec{r}_i = (x_i, y_i, z_i)$ in the Cartesian coordinate system. We also use local frames attached to molecules. In this case the z axis in Eq. (5) is set along the long axis of the molecule and we label the corresponding coordinates and variables with the superscript (l) .

Molecules, positioned at points $\vec{r}_i(t)$, are allowed to wander around the points of the three dimensional hexagonal lattice with spacing a_o . By such a box restricted dynamics we get rid of the lattice induced ordering anisotropy known to appear in the cubic lattice [20,23,24]. The amplitude $\Delta r = |\Delta \vec{r}_i|$ of isotropic random wandering is distributed by the Gaussian distribution centered at $\Delta r = 0$ whose width depends on temperature T . In our simulations the results, relatively, weakly depend on a specific choice of parameters characterizing the distribution Δr .

The cylinder radius is set to $R = N_r a_o$. At a distance $L = N_z a_o$ along the cylinder axis the periodic boundary conditions are imposed simulating an infinite cylindrical capillary. Here N_r and N_z are positive integers.

The local frame molecular orientation is updated at each point i in a time interval Δt [29] according to

$$\Theta^{(l)}(\vec{r}_i, t + \Delta t) = \Theta^{(l)}(\vec{r}_i, t) - \sum_{j \neq i} \frac{D_{ij}^{(l)}}{kT} \Delta t \frac{\partial f_{ij}}{\partial \Theta^{(l)}} + \Theta_{r,i}^{(l)}, \quad (6a)$$

$$\Phi^{(l)}(\vec{r}_i, t + \Delta t) = \Phi^{(l)}(\vec{r}_i, t) - \sum_{j \neq i} \frac{D_{ij}^{(l)}}{kT} \Delta t \frac{\partial f_{ij}}{\partial \Phi^{(l)}} + \Phi_{r,i}^{(l)}. \quad (6b)$$

k stands for the Boltzmann constant, $D_{ij}^{(l)}$ is the rotational diffusion tensor, and $\Theta_{r,i}^{(l)}$ and $\Phi_{r,i}^{(l)}$ are stochastic variables obeying the Gaussian distribution. The corresponding probabilities are centered at $\Theta_{r,i}^{(l)} = 0$ and $\Phi_{r,i}^{(l)} = 0$ and the width of the distribution is proportional to \sqrt{T} . The rotations corresponding to $\Delta \Theta^{(l)} = \Theta^{(l)}(\vec{r}_i, t + \Delta t) - \Theta^{(l)}(\vec{r}_i, t)$ and $\Delta \Phi^{(l)} = \Phi^{(l)}(\vec{r}_i, t + \Delta t) - \Phi^{(l)}(\vec{r}_i, t)$ are mutually perpendicular and also perpendicular to $\vec{e}_z^{(l)}$. The tensor $D_{ij}^{(l)}$ is diagonal in the local frame. The eigenvalues are assumed to be degenerated and equal to D . The shortest time interval Δt_0 of the model in the simulation is set by $\Delta t_0 D \sim 0.01$. For a typical nematic LC this ranges within the interval $\Delta t_0 \sim 0.001 \mu s$ to $\Delta t_0 \sim 0.1 \mu s$ depending on the size of a molecule. An estimate of a Δt_0 value was obtained by comparing a response of the system to an external perturbation calculated from the semimicroscopic and the continuum-type approach [30].

In the simulation either the strong *homeotropic* ($|\vec{e}_s \cdot \vec{e}_v| = 1$), *tangential* ($\vec{e}_s \cdot \vec{e}_v = 0$), or *tilted* ($1 > |\vec{e}_s \cdot \vec{e}_v| > 0$) surface anchoring [26] is used. Here \vec{e}_v points along a surface normal. The easy axis \vec{e}_s defines the orientations of nematic molecules at the surface that minimize the surface free energy contribution. Simulations are performed for $2N_r$ between 16 to 54 and N_z between 44 to 96. The anisotropy parameter is set to $\varepsilon = 0.1$. The liquid crystal was first equilibrated in the isotropic phase and then suddenly cooled deep into the nematic phase.

C. Characteristic parameters

We first introduce semimesoscopic parameters revealing essential properties of our nematic textures. Going beyond the simple picture used in Sec. II, local properties at a site $\vec{r} = \vec{r}_i$ are described by the mesoscopic nematic order parameter [5]

$$Q(\vec{r}) = \frac{1}{2} \langle 3\vec{e}_i \otimes \vec{e}_i - \mathbf{I} \rangle = \frac{S}{2} (3\vec{n} \otimes \vec{n} - \mathbf{I}) + P(\vec{l} \otimes \vec{l} - \vec{m} \otimes \vec{m}). \quad (7a)$$

The triad \vec{n} , \vec{l} , and \vec{m} defines the Q eigenvectors, the eigenvalues of which are expressed with the uniaxial (S) and the biaxial (P) order parameter. The local time-and-space averaging is denoted by $\langle \dots \rangle$. The local spatial averaging is performed by taking into account the neighbors within a sphere of the radius a_0 . The time averaging is calculated within the time $t_a \sim 10\Delta t_0$. This time interval is long enough so that we obtain $S \sim 0$ in the isotropic phase. The eigenframe and the corresponding values of $S(\vec{r})$ and $P(\vec{r})$ were obtained via diagonalization of $Q(\vec{r})$ at each lattice point. We introduce also the corresponding global spatially averaged values of the order parameters \bar{S} and \bar{P} obtained by averaging over all sites of the lattice.

In order to monitor the time evolution of nematic textures we introduce the average projection P_{2z} of the nematic ordering on the cylinder symmetry axis and the average domain size ξ_d . The quantity P_{2z} is defined as

$$P_{2z} = \frac{1}{2} [3(\vec{e}_i \cdot \vec{e}_z)^2 - 1]. \quad (7b)$$

Thus $P_{2z} = 1$, $P_{2z} = -0.5$, and $P_{2z} = 0$ correspond to a homogeneously aligned structure along the z axis, radially aligned structure in the (x, y) plane [see Eq. (5)], and isotropic distributions of \vec{e}_i , respectively.

We estimate a typical linear size ξ_d of an average domain of a texture after the quench using two criteria, one based on the geometry and the other on energy of domains. In the first case we obtain ξ_d directly from a nematic pattern. For this purpose we calculate at the time t an average volume V_d in which only relatively small changes of the orientational ordering occur. As the criterion of being in a domain we chose $|\cos \Theta_{i,i+1}| = |\vec{e}_i \cdot \vec{e}_{i+1}| > 1 - \Delta$, where $\Theta_{i,i+1}$ is a relative angle between a pair of adjacent molecules. In the simulations we set $\Delta \sim 0.2$ corresponding to the amplitude of thermal fluctuations at approximately double width of the Gaussian distribution. The domain size is then estimated as

$$\xi_d^{(g)} \sim \left(\frac{3V_d}{4\pi} \right)^{1/3}. \quad (8a)$$

In expressing the domain size on energy grounds we start with the excess free energy $\Delta F = F(t) - F_{\text{eq}}$. Here $F(t)$ is the free energy of the system at the time t and $F_{\text{eq}} = F(t \rightarrow \infty)$. We then assume that all energy contributions come from the domain walls [i.e., $f_A = f_B$ in Eq. (3)]. Consequently the average excess free energy of a volume V is roughly given by $\Delta f = \Delta F/V \sim f_w V_w/V_d$. The quantity f_w estimates

a deformation average free energy cost of a domain wall, $V_d \sim \xi_d^3$ is the average domain volume, and $V_w \sim \xi_d^2 d_w$ is the average volume of the domain wall. With this in mind [1,20] one finds for the domain size

$$\xi_d^{(F)} \sim \frac{c}{\Delta f}, \quad (8b)$$

where c is a constant. In the numerical simulation we determine a value of c from an average domain size of a nematic pattern at an arbitrary time.

The superscripts (g) and (F) in Eqs. (8a) and (8b) remind us that the domain size was obtained on geometry and energy grounds, respectively.

IV. SIMULATION RESULTS

A. Confinement: Equilibrium structures

An important parameter of our study is the final nematic equilibrium structure. For a given confinement it reflects the interplay between the elastic and surface interactions. In the following we describe the structures that enter our study. The corresponding figures of structures are shown in the nematic director field representation (Fig. 2).

The stability diagram of nematic structures confined to an infinite cylindrical capillary with *homeotropic* anchoring was discussed in detail in Refs. [25,31]. In our study we focus to the conditions where either the *escaped radial* (ER) or the *planar polar structure with line defects* (PPLD) [25,31] is stable. In the ER structure the molecules orientated along the cylinder axis at the cylinder center gradually reorient towards the radial orientation as the cylinder's lateral wall is approached [Fig. 2(a)]. In the PPLD structure [Fig. 2(b)] the molecules are constrained to the azimuthal plane [the (x,y) plane according to Eq. (5)]. Close to the cylinder axis molecules are preferentially aligned along a symmetry breaking direction. In order to fulfill strong homeotropic anchoring at the cylinder wall two line defects parallel to the cylinder axis are formed. The ER structure is stable for $R \geq R_c$ [32] and the PPLD structure for $R \leq R_c$. The critical value R_c depends on temperature, anchoring strength, and LC elastic properties [25]. In the strong anchoring regime and deep in the nematic phase $2R_c/a_o$ is between 44 and 54 for $\varepsilon=0.1$.

We further limit ourselves to the regime where the ER structure is stable for strong homeotropic anchoring (i.e., $\vec{e}_s \cdot \vec{e}_z = 0$). Note that in this structure the director field avoids singularity at the cylinder axis by “escaping” along the z direction [32]. Because both directions (i.e., $\pm \vec{e}_z$) of the escape are equivalent the corresponding free energies are the same. If, however, a finite tilt ϑ_t from the surface normal is imposed, defined by $\cos[(\pi/2) - \vartheta_t] = \vec{e}_s \cdot \vec{e}_z$, the degeneracy is lifted in favor of the escape along $-\vec{e}_z$ for $\vartheta_t > 0$. We refer to the resulting structure for $\pi/2 > \vartheta_t > 0$ as the ER-like one, with a typical representative shown in Fig. 2(c). For $\vartheta_t = \pi/2$ the tangential boundary condition is realized enforcing a homogeneously aligned structure along the cylinder axis. Note that the ER-like structure can be stable also in the regime $R < R_c$ for a large enough tilt angle ϑ_t .

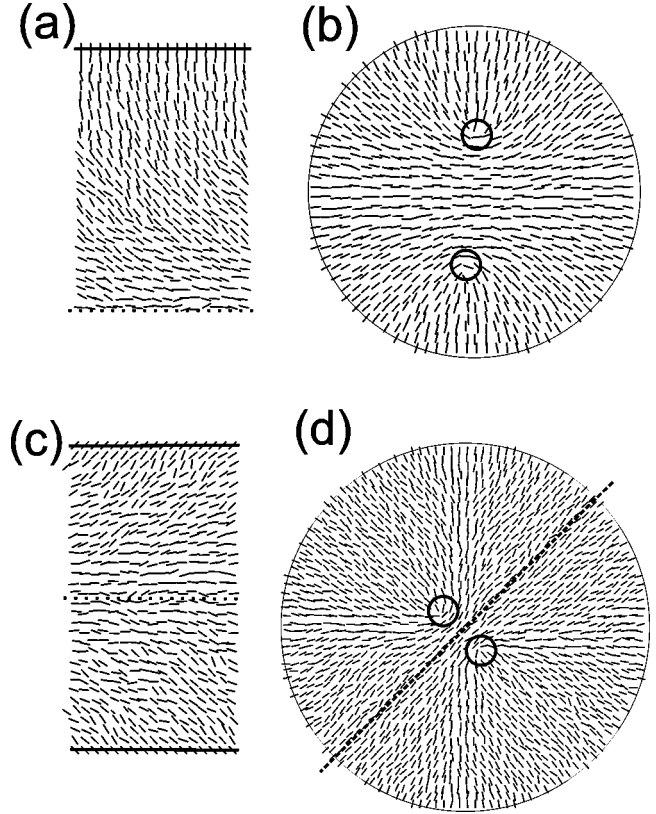


FIG. 2. Possible nematic ground state structures in the cylindrical (a)–(c) and spherical (d) confinement. The representative cross sections are shown to which the molecules are restricted on the average. (a) The escaped radial structure (ER). The (y, z) cross section: full line, the cylinder wall; dotted line, the cylinder axis. (b) The planar polar structure (PPLD). The (x, y) cross section: full line, the cylinder wall. The small circles indicate line defects running along the cylinder axis. (c) The ER-like structure. The (y, z) cross section: full line, the cylinder wall; dotted line, the cylinder axis. (d) The radial structure with a ringlike point defect. The structure is shown in the cross section through the center of the confining sphere that lies perpendicular to the ring of the point defect. The dotted line indicates the rotational symmetry axis of the structure and the small circles indicate the location of the defect.

For the spherical confinement we limit to a large enough spherical cavity (with respect to a typical nematic order parameter correlation length) and strong homeotropic anchoring. In this case the *radial* structure [33,34] is realized in which the director field radially streams from the center where a *point* defect is located. The resulting structure exhibits a spherical symmetry only for defects with the uniaxial core structure. In this case the center of defect is melted. This core structure is realized only for $T \sim T_{NI}$ and for a certain anisotropy of Frank elastic constants [35,36]. In general the *point* defect is broadened into a *ring* where LC locally exhibits biaxial ordering. The details of the *ring* structure are given in Ref. [36]. The ring radius is comparable to the nematic biaxial correlation length [36]. The resulting structure in the nematic director field representation is shown in Fig. 2(c).

B. Quench induced kinetics

We next follow kinetics after a sudden quench from the isotropic to the N phase of a confined LC. These simulations mimic the regime where the quench time is short in comparison to the characteristic relaxation time of nematic fluctuations. In this study we focus to the influence of a confinement geometry and boundary conditions. In order to point out the influence of confinement on the pattern evolution we first analyze the bulk behavior.

1. Quench kinetics in bulk

We simulate a *bulk* sample by enclosing a LC in a cube of length R_p and impose periodic boundary conditions at its surface. We checked the annealing kinetics for different values of R_p to verify that the choice of R_p does not introduce an additional length scale into the model. The main results of simulations are summarized in Figs. 3. We plot the time evolution of a typical domain size ξ_d and of the spatially averaged uniaxial nematic order parameter \bar{S} .

The annealing kinetics in bulk exhibits three qualitatively different stages. The *early regime* is dominated by the growth of a long wave fluctuation mode of S . This mode tends to establish spatially homogeneous structure with $S(\vec{r}) \sim S_b$. In this regime the order parameter [Fig. 3(a)] exhibits the exponential growth in accordance with our estimate Eq. (2) and lasts till the so-called *Zurek* time [9] $t_z \gtrsim \tau_0$. At this time \bar{S} becomes comparable to its equilibrium value and the domains just become apparent.

The second regime, which we call the *domain regime*, is characterized by a multidomain structure. The domain structure at different times is visible in Fig. 4. Their size distribution seems to be relatively sharp. With increased time larger domains, which have a lower free energy because of larger volume with relatively uniformly aligned molecules, progressively grow on expense of smaller domains. The corresponding $\xi_d(t)$ dependence monotonically grows with time. In this regime the scaling regime is entered where the initial details of the quench are forgotten. The scaling law $\xi_d \propto t^\gamma$ is well obeyed, as shown in Fig. 3(c). The scaling factor value $\gamma \sim 0.47 \pm 0.05$ is in agreement with the estimate Eq. (3) providing that the main driving mechanism is the tendency to reduce the overall surface of domain walls. Further support for this conclusion is the excellent match of $\xi_d(t)$ dependencies calculated using the *excess energy* [$\xi_d^{(F)}$, Eq. (8b)] and the *geometrical* [$\xi_d^{(g)}$, Eq. (8a)] method described in Sec. III C.

In the third regime, to which we refer as the *late stage* regime, the structure of individual defects begins to dominate the nematic pattern. In this regime domains are not any more well defined and ξ_d now better represents an average separation between neighboring defects. Finally this regime ends in the defectless nematic structure.

2. Quench kinetics in confined samples

In practice the I - N quench is always realized within a cavity. As already shown by Bhattacharya *et al.* [10] an additional qualitative change of behavior in comparison to the

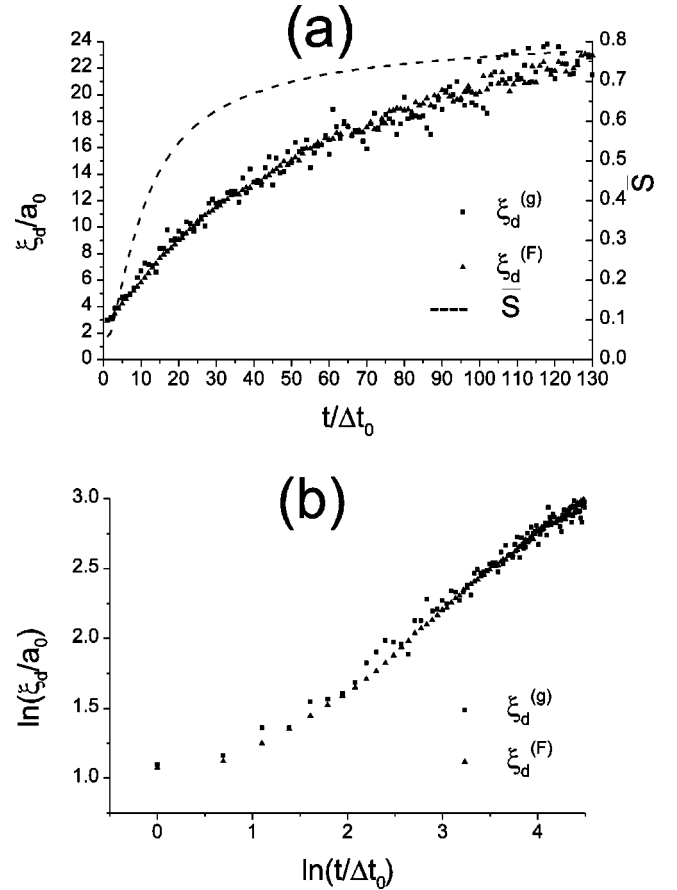


FIG. 3. (a) The time evolution of the average domain size $\xi_d(t)$ and the average nematic order parameter \bar{S} in a bulk nematic texture. The $\xi_d(t)$ dependence is calculated using the excess energy ($\xi_d^{(F)}$) and geometry ($\xi_d^{(g)}$) grounds. In calculation we use a cubic sample with the typical length $44a_0$ and periodic boundary conditions. (b) The log-log diagram reveals the scaling law $\xi_d(t) \sim t^\gamma$ and $\gamma = 0.47 \pm 0.05$.

bulk scenario is expected when ξ_d becomes comparable to the shortest typical linear dimension of the confining cavity.

We first follow the quench induced kinetics in the cylindrical confinement. In Fig. 5(a) we plot the $\xi_d(t)$ dependence for three different values of R for strong homeotropic anchoring. For $R < R_c$ (cases $2N_r = 16$ and 30) the PPLD structure is stable and the ER one for $R > R_c$ (case $2N_r = 54$). One sees a qualitative change at the crossover time t_c , which is roughly determined by the condition $\xi_d(t = t_c) \sim R$. The time t_c helps us to distinguish between the bulk and the *confinement* regime. In the first regime the domain growth is only weakly influenced by the confinement and consequently the scaling law $\gamma \sim 0.49 \pm 0.05$ is similar (slightly different) as in the bulk. In the *confinement* regime the qualitative change of the scaling law is observed due to the restricted domain growth along the cylinder symmetry axis. We obtain $\gamma \sim 0.25 \pm 0.05$ and $\gamma \sim 0.12 \pm 0.02$ for the PPLD and ER scenario, respectively. In the ER scenario the domain growth is apparently slower due to the competition between the two degenerate ER solutions, corresponding to the escapes along \vec{e}_z and $-\vec{e}_z$, respectively.

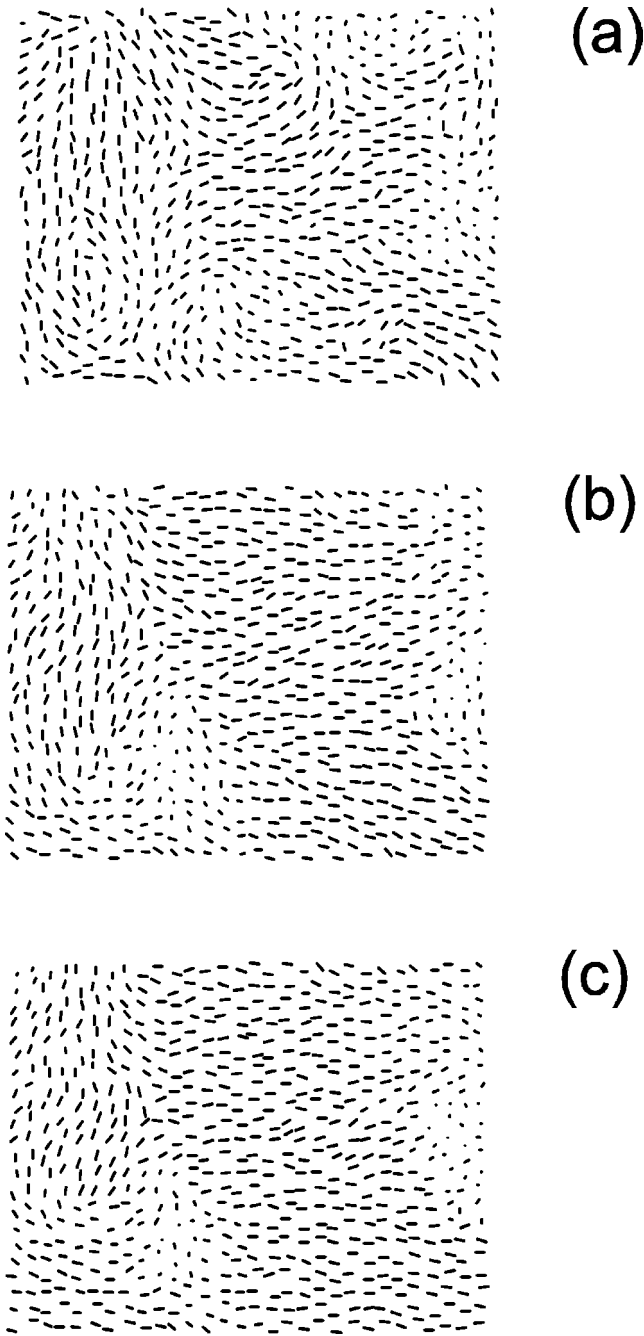


FIG. 4. The multidomain structure of a nematic texture for different times after the I - N quench. A point corresponds to a molecule pointing out of the plane. (a) $t=40\Delta t_0$, (b) $t=80\Delta t_0$, (c) $t=120\Delta t_0$.

The effect of the anchoring on the kinetics can be inferred from Fig. 5(b). The cases of homeotropic ($\vartheta_t=0$), conic ($\vartheta_t=\pi/4$), and tangential ($\vartheta_t=\pi/2$) anchorings are shown leading to the PPLD the ER-like, and the homogeneously aligned structure along the z axis, respectively. The typical time to achieve the equilibration is the shortest for the *tangential* and the longest for the homeotropic anchoring. In the homeotropic anchoring case the surface does not prefer any direction along the cylinder axis that results in a relatively slow decay. In the *tilted* case the ER-like structure is stable.

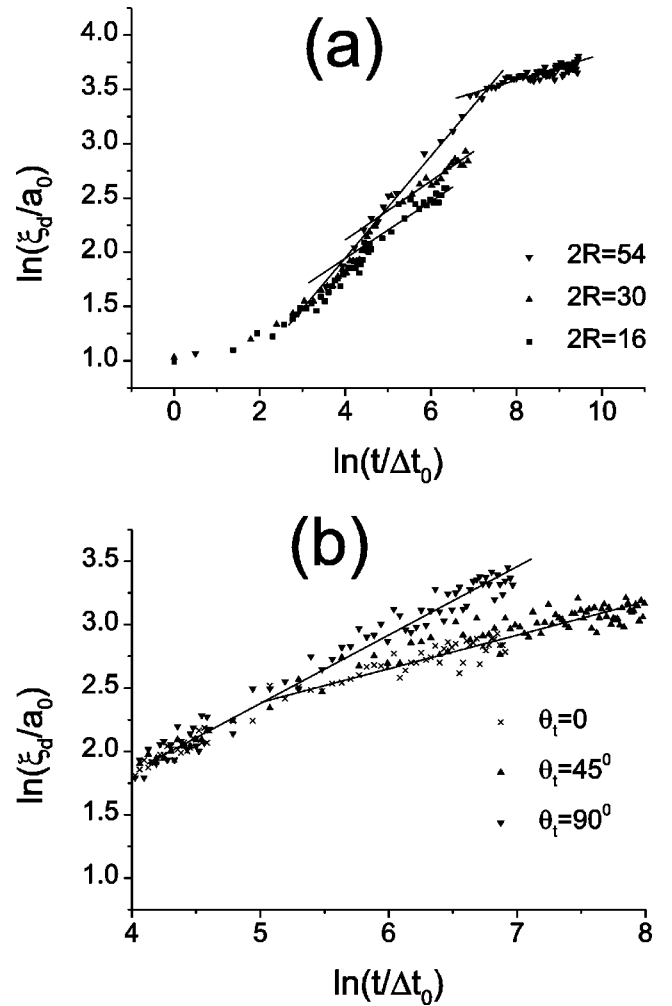


FIG. 5. Influence of cylindrical confinement on the $\xi_d(t)$ dependence. The full lines are guides for the eye, $N_z=96$ and $\varepsilon=0.1$. (a) Dependence on the cylinder radius R for the homeotropic anchoring: $2N_r=16$, the PPLD structure; $2N_r=44$, the PPLD structure; and $2N_r=54$, the ER structure. The bulk regime: $\gamma=0.49\pm 0.05$; the confinement regime: $\gamma(\text{PPLD})=0.25\pm 0.05$, $\gamma(\text{ER})=0.12\pm 0.02$. (b) Effect of boundary conditions on $\xi_d(t)$, $2N_r=30$. The cases of homeotropic ($\vartheta_t=0$), conic ($\vartheta_t=\pi/4$), and tangential ($\vartheta_t=\pi/2$) anchorings are shown. The corresponding equilibrium profiles are PPLD, ER-like, and the homogeneously aligned structure along the z axis, respectively. $\gamma(\vartheta_t=\pi/4, 2N_r=30, \text{ER-like})\sim\gamma(\vartheta_t=0, 2N_r=30, \text{PPLD})\sim 0.25\pm 0.05$, $\gamma(\vartheta_t=\pi/2, 2N_r=30, \text{homogeneous})\sim 0.52\pm 0.05$.

The surface imposed tilt acts as an effective field giving preference to the “escape” along a single direction. Note that the structure with the “escape” along the opposite direction still exist as a metastable solution. For the tangential anchoring condition only one final solution exists resulting in the fastest equilibration after the quench. It is to be stressed that for $\vartheta_t>0$ the scaling coefficient also depends on the cavity size. With decreasing radius R the influence of surface induced effective field is increasing and consequently also a value of γ . For chosen examples we get the following values of the scaling coefficient: $\gamma(\vartheta_t=\pi/2, 2N_r=16, \text{homogeneous})=0.85\pm 0.05$, $\gamma(\vartheta_t=\pi/2, 2N_r=30, \text{homogeneous})=0.52\pm 0.05$, $\gamma(\vartheta_t=\pi/4, 2N_r=30, \text{ER-like})=0.25\pm 0.05$, and $\gamma(\vartheta_t=0, R>R_c, \text{ER})=0.12\pm 0.02$. Therefore, in the con-

finement regime the scaling coefficient strongly depends on the confinement details and is far from being determined by the space and order parameter dimensionality.

In Fig. 6 we simulate the annealing kinetics in the spherical confinement. The equilibrium nematic director profile is the radial one, shown in Fig. 2(d). As expected in the spherical confinement the domain growth is after the time $t > t_c$ restricted in all directions with the cavity size, evidently shown in Fig. 6(a). But the approaching towards the final equilibrium structure is not so trivial. This evolution is for $t > t_c$ monitored by observing the time dependence of the radius R_d of the ring defect. At $t \sim t_c$ a monodomain structure is formed characterized by a relatively broad ring of radius $R_d \sim R/2$, shown in Fig. 6(b). With increasing time the ring gradually shrinks [Fig. 6(c)] asymptotically approaching its equilibrium size. Note that the equilibrium ring size is comparable to the nematic biaxial correlation length yielding a further gauge for the system sizes used in the simulations [34].

V. CONCLUSIONS

We study the influence of confinement on the kinetics of a temperature driven I - N quench. The semimicroscopic model is used in which molecules interact via a modified induced-dipole–induced-dipole interaction. The dynamics of the system is followed using the Brownian molecular dynamics. This approach enabled us to study phenomena on macroscopic time scales that is necessary to follow the evolution towards equilibrium states. The liquid crystal molecules are also allowed to wander around the sites of a hexagonal lattice of lattice spacing a_0 . Consequently preferred directions in the model induced by a specific choice of a lattice are averaged out. A molecule of the model corresponds to a cluster of N_c molecules where N_c is estimated to be less or equal to the number of neighbors [25,28] within a sphere of radius a_0 , i.e., $N_c \leq 26$. The time step of the simulation strongly depends on the size of a molecule and with this respect ranges within the interval $\Delta t_0 \sim 0.001 \mu\text{s}$ to $\Delta t_0 \sim 0.1 \mu\text{s}$. The estimates for (i) N_c and (ii) Δt_0 were obtained by comparing (i) the defect core size of a point defect of the radial structure and (ii) the relaxation rate of a twist induced distortion in a plane-parallel cell obtained by our simulation with the result of the analogous continuum-type calculation [30,36]

In the simulations we limit to a sudden quench. In practice this mimics the quench that is realized fast with respect to a typical nematic order parameter relaxation time. The results indicate several qualitatively different stages of the annealing process after the quench.

In bulk we distinguish between the *early, domain*, and *late stage* regime. The early regime is dominated by the exponential growth of the nematic uniaxial order parameter. At the end of it domains are formed that are easily recognizable in the domain regime. With time the nematic texture gradually enters the late stage regime dominated by structures of individual defects. After the early regime the domain growth exhibits to a good approximation the scaling law $\xi_d \sim t^\gamma$, $\gamma = 0.47 \pm 0.05$. A similar result was obtained by Bhattacharya

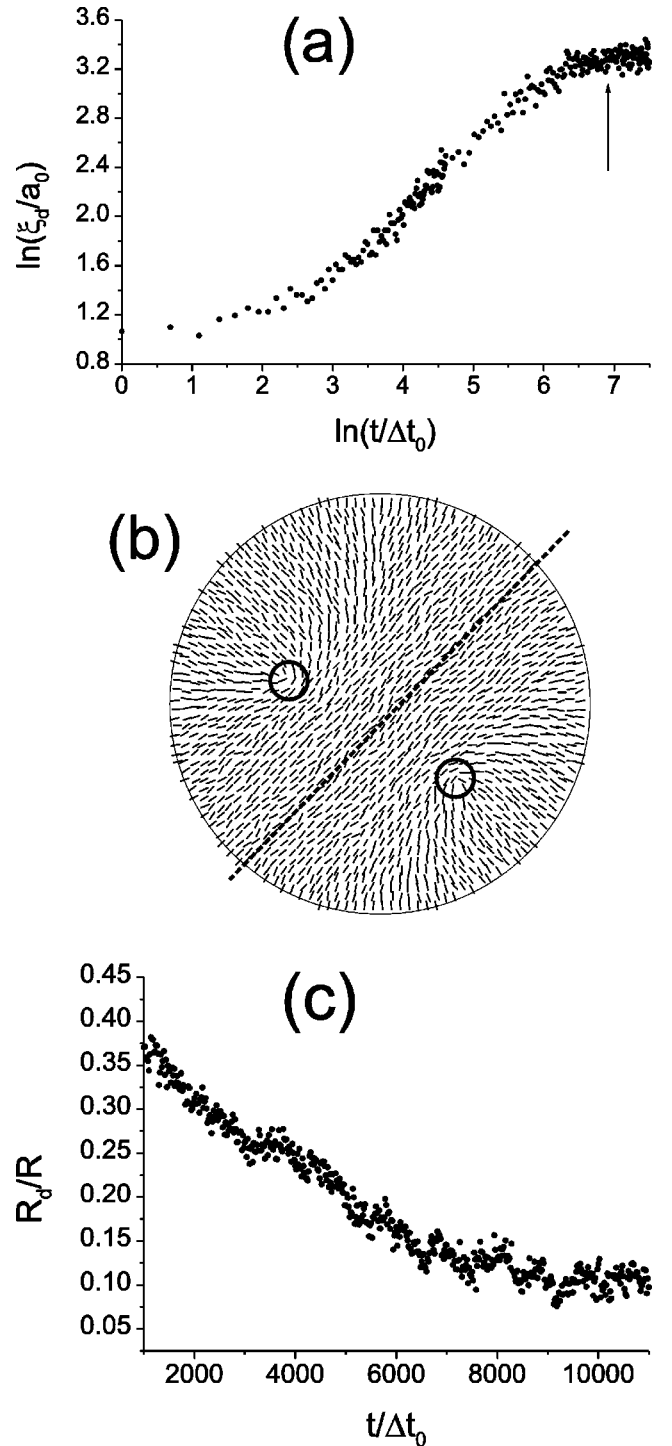


FIG. 6. The annealing kinetics in the spherical confinement $2N_r=44$ and $\varepsilon=0.1$. The time evolution of (a) ξ_d and (c) of the ring radius R_d . The ring appears in the confinement regime. Its evolution is monitored above the time depicted by the arrow in (a). The structure at the time indicated by the arrow is shown in (b) and the equilibrium structure in Fig. 2(d). In (a) and (b) the small circles locate the ring of the defect.

et al. [10] within a simple continuum Langevin approach yielding $\gamma=0.45 \pm 0.02$. Almost identical values of γ obtained via different approaches indicate that results are rather weakly sensitive to the details of the model.

In confined samples an additional qualitative change of the behavior appears when ξ_d becomes comparable to the typical linear size R of the system [10]. The condition $\xi_d \sim R$ roughly distinguishes between the bulk ($\xi_d < R$) and confinement ($\xi_d > R$) regime. Only in the latter regime are apparent departures from the bulk behavior observed. The scaling coefficient now reflects confinement details and also a final equilibrium director structure. The scaling exponent changes from $\gamma = 0.49 \pm 0.05$ in the bulk regime to $\gamma = \gamma(\vartheta_t, R)$ (equilibrium structure) in the confinement regime. For the cylindrical confinement we obtain either slower [e.g., $\gamma(\vartheta_t = \pi/4, 2N_r = 30, \text{ER-like}) \sim 0.25 \pm 0.05$ and $\gamma(\vartheta_t = 0, 2N_r = 54, \text{ER}) \sim 0.12 \pm 0.02$] or faster [e.g., $\gamma(\vartheta_t = \pi/2, 2N_r = 16, \text{homogeneous}) \sim 0.85 \pm 0.05$, $\gamma(\vartheta_t = \pi/2, 2N_r = 30, \text{homogeneous}) \sim 0.52 \pm 0.05$] domain growth with respect to the *bulk* regime.

For $\vartheta_t = 0$ the effective field in the direction of the domain growth is not present. In the late stage regime the domain growth is restricted along the cylinder symmetry axis. This does not significantly reduce the overall size of domain walls until a disappearance of a less favored domain. In this case the main driving mechanism is the difference in the free energy between neighboring domains that in general changes with time. If this difference is small enough the structure can freeze. In practice this often happens for the case of homeotropic anchoring in the regime, where the escaped radial structure corresponds to the ground state. However, often the escaped radial structure with point defects is realized instead [37] characterized by domains with the ER-like profile with alternative preferred orientation along the cylinder axis.

Our results confirm that the domain growth is well described with the *Kibble-Zurek mechanism* [3,9]. This mechanism was originally introduced in cosmology to explain the

formation of topological defect in the early Universe. Based on simple causality arguments it yields estimates of the domain density and consequently defects (i.e., vortex lines or strings) produced in the phase transitions in which a continuous symmetry of the relevant order parameter field is broken. In a nematic LC phase an additional source [21,22] of defects could arise due to topological constraints at the domain wall boundary. In case of strong tangential or homeotropic anchoring they would, e.g., enforce defects with total bulk charge $M=2$ or $M=1$, respectively. But this source of defects becomes effective when the condition $W_a^{(\text{intrinsic})} \xi_d / K \gg 1$ is realized. For most nematic LCs this condition would be fulfilled in a relatively late stage of the texture evolution in case of appropriate conditions at a domain wall. In our simulation this source of defects was not observed. It might be important in the temperature regime where the isotropic phase is still metastable.

In our theoretical study we considered a sudden temperature quench. In reality this mimics well a case when the quench is realized in a short time scale in comparison to a relevant order parameter relaxation time. In the case of a nematic liquid crystal this condition is relatively hard to realize. For this purpose we will focus in our future study on the influence of quench rate on the nematic texture evolution. This study would be of particular interest because of its relevance to other fields of physics, particularly cosmology.

ACKNOWLEDGMENTS

This research was supported by a bilateral cooperation between Austria and Slovenia (SLO-A/11), ESF network Project No. COSLAB, and Slovenian Office of Science (Research Program No. PO-0524-0106).

-
- [1] A. Sadiq and K. Binder, *J. Stat. Phys.* **35**, 517 (1984).
 [2] I. Chuang, B. Yurke, A. Pargellis, and N. Turok, *Phys. Rev. E* **47**, 3343 (1993).
 [3] T. W. B. Kibble, *J. Phys. A* **9**, 1 (1976).
 [4] N. D. Mermin, *Rev. Mod. Phys.* **51**, 591 (1976).
 [5] P. G. de Gennes and J. Prost, *The Physics of Liquid Crystals* (Oxford University Press, Oxford, 1993).
 [6] M. Kleman, *Points, Lines and Walls* (Wiley, Chichester, 1983).
 [7] M. V. Kurik and O. D. Lavrentovich, *Usp. Fiz. Nauk* **154**, 381 (1988) [*Sov. Phys. Usp.* **31**, 196 (1988)], and references therein.
 [8] O. D. Lavrentovich, *Liq. Cryst.* **24**, 117 (1998).
 [9] W. H. Zurek, *Phys. Rep.* **276**, 178 (1996).
 [10] A. Bhattacharya, M. Rao, and A. Chakrabarti, *Phys. Rev. E* **53**, 4899 (1996).
 [11] R. A. Wickham, *Phys. Rev. E* **56**, 6843 (1997).
 [12] K. Minoura, Y. Kimura, K. Ito, R. Hayakawa, and T. Miura, *Phys. Rev. E* **58**, 643 (1998).
 [13] J. L. Billeter, A. M. Smondyrev, G. B. Loriot, and R. A. Pelcovits, *Phys. Rev. E* **60**, 6831 (1999), and references therein.
 [14] G. S. Iannacchione, J. T. Mang, S. Kumar, and D. Finotello, *Phys. Rev. Lett.* **73**, 2708 (1994).
 [15] R. J. Ondris-Crawford, G. P. Crawford, J. W. Doane, S. Žumer, M. Vilfan, and I. Vilfan, *Phys. Rev. E* **48**, 1998 (1993).
 [16] G. S. Iannacchione, G. P. Crawford, S. Žumer, J. W. Doane, and D. Finotello, *Phys. Rev. Lett.* **71**, 2595 (1993).
 [17] M. Dadmun and M. Muthukumar, *J. Chem. Phys.* **97**, 578 (1992).
 [18] S. Kralj, A. Zidanšek, C. Lahajnar, S. Žumer, and R. Blinc, *Phys. Rev. E* **62**, 718 (2000).
 [19] S. Kralj and S. Žumer, *Phys. Rev. E* **51**, 366 (1995).
 [20] J. Ding and Y. Yang, *Liq. Cryst.* **25**, 101 (1998).
 [21] V. Popa-Nita and T. J. Sluckin, *J. Phys. II* **6**, 873 (1996), and references therein.
 [22] O. D. Lavrentovich and E. M. Terentjev (unpublished).
 [23] G. Barbero, *Mol. Cryst. Liq. Cryst.* **195**, 199 (1991).
 [24] G. Skačej, V. M. Pergamenschchik, A. L. Alexe-Ionescu, G. Barbero, and S. Žumer, *Phys. Rev. E* **56**, 571 (1997), and references therein.
 [25] Z. Bradač, S. Kralj, and S. Žumer, *Phys. Rev. E* **58**, 7447 (1998).
 [26] B. Jerome, *Rep. Prog. Phys.* **54**, 351 (1991), and references therein.
 [27] E. Berggren, C. Zannoni, C. Chiccoli, P. Pasini, and F. Seme-

- ria, Phys. Rev. E **50**, 2929 (1994).
- [28] T. Bellini, C. Chiccoli, P. Pasini, and C. Zannoni, Mol. Cryst. Liq. Cryst. Suppl. Ser. **290**, 227 (1996).
- [29] D. L. Ermak, J. Chem. Phys. **62**, 4189 (1975).
- [30] Z. Bradač, S. Kralj, and S. Žumer (unpublished).
- [31] A. Sonnet, A. Kilian, and S. Hess, Phys. Rev. E **52**, 718 (1995).
- [32] C. Williams, P. Pieranski, and P. E. Cladis, Phys. Rev. Lett. **29**, 90 (1972).
- [33] N. Schopol and T. J. Sluckin, J. Phys. (France) **49**, 1097 (1988).
- [34] S. Kralj, S. Žumer, and D. W. Allender, Phys. Rev. A **43**, 2943 (1991).
- [35] R. Rosso and E. G. Virga, J. Phys. A **29**, 4247 (1996).
- [36] S. Kralj, E. G. Virga, and S. Žumer, Phys. Rev. E **60**, 1858 (1999).
- [37] G. G. Peroli and E. G. Virga, Phys. Rev. E **59**, 3027 (1999).